Chapter 3

Magnetic Properties of the Size-Controlled Mn-Zn Ferrite Nanoparticles

3.1. Introduction

Ferrite nanoparticles find important applications in heat transfer devices, drug delivery systems and in medical diagnostics [1-4]. Nanosize particles of ferrites can be prepared using various synthesis techniques namely, ballmilling [5], citrate precursor [6], hydrothermal [7], coprecipitation [8,9] and other chemical methods [10]. Coprecipitation technique has been employed to synthesize nanoparticles below 25 nm in some ferrites like $MnFe_2O_4$ [11], $CdFe_2O_4$ [12] and $MgFe_2O_4$ [13]. However, the preparation of nonagglomerated size-controlled particles with large diameters still remains a challenge. Tamura and Matijevic [14] have synthesized ferrite particles using the oxidation method with an emphasis on the shape rather than the size of the particles. The maximum size that could be achieved, so far, for the Mn-Zn ferrite nanoparticles synthesized using oxidation method is 20 nm only [15]. But a modified oxidation method yields particles of size as large as 100 nm in $CoFe_2O_4$ where the nucleation rate is controlled by varying the concentration of ferric ions [16].

The saturation magnetization of the nanoparticles decreases due to surface spin effects when the particle size is decreased to a few nanometer [17]. The magnetic anisotropy of the smaller particles is found to increase due to surface anisotropy according to the relation $H_s = 6h_s D^{-\alpha}$ where H_s is the surface anisotropy field coefficient, h_s is the surface anisotropy field, D is the particle diameter and α is a constant close to unity [18,19]. The increase in the effective magnetic anisotropy due to surface anisotropy has been reported in some ferrite nanoparticles like $CoFe_2O_4$ [20], Fe_3O_4 [21] and γ-Fe_2O_3 [22] where it is one or two orders higher than that of their bulk counterpart. This chapter deals with the magnetic properties of Mn-Zn ferrite nanoparticles synthesized using the oxidation method with a wide range of particle size with an emphasis on the determination of the effective magnetic anisotropy.

3.2. Experiment

$Mn_{0.67}Zn_{0.33}Fe_2O_4$ was synthesized using analytical grade reagents of $FeSO_4.7H_2O$, $MnCl_2.4H_2O$, $ZnSO_4.H_2O$ and $Fe_2(SO_4)_3$ salts, wherever necessary, fixing the ratio of Mn to Zn as 2. NaOH was used for the metal hydroxide precipitation and KNO_3 was used to oxidize the ferrous ions to the ferric state. The Fe, Mn and Zn salts were dissolved separately in water (250 mL) and NaOH was also dissolved in an equal amount of water. The solutions were purged with N_2 for 30 min before mixing and heating. The metal hydroxide precipitate with a pH between 12-13 was oxidized with various amounts of KNO_3 in a round bottom flask at 363 K under constant mechanical stirring for 2 h. The resulting ferrite precipitate was washed several times with water and dried in an oven at 333 K for 48 h. While using ferric salts, a suitable percentage of ferric salt was taken along with the ferrous salt and the same procedure as that followed in the oxidation method was adopted. The crystallographic phase analysis was carried out using an RIGAKU X-ray diffractometer with Cu K_α radiation. The average grain size was calculated from the width of the (311) peak using the Scherrer formula. The average particle size was examined using a scanning electron microscope (SEM) and also a transmission electron microscope (TEM). The magnetic properties were studied using a Tamakawa VSM in a maximum applied field of 1 T. The Mössbauer spectra were recorded using a Wiessel constant acceleration Mössbauer spectrometer with a ^{57}Co/Rh source kept at 293 K. The low-temperature Mössbauer experiments were performed from 293 to 16 K using a closed cycle helium cryostat.

3.3. Results and Discussion

3.3.1. The size controlled synthesis of Mn-Zn ferrite

The slow oxidation of the hydroxide precipitate with a mild oxidant such as KNO_3 was used to oxidize the ferrous ions. The amount of KNO_3 used for the rate of generation of ferric ions determines the final particle size of the ferrites as in the case of other oxidants like air and H_2O_2 [15, 23]. Another method used to prepare larger particles is to introduce ferric ions along with ferrous ions at the beginning of the reaction itself thereby separating

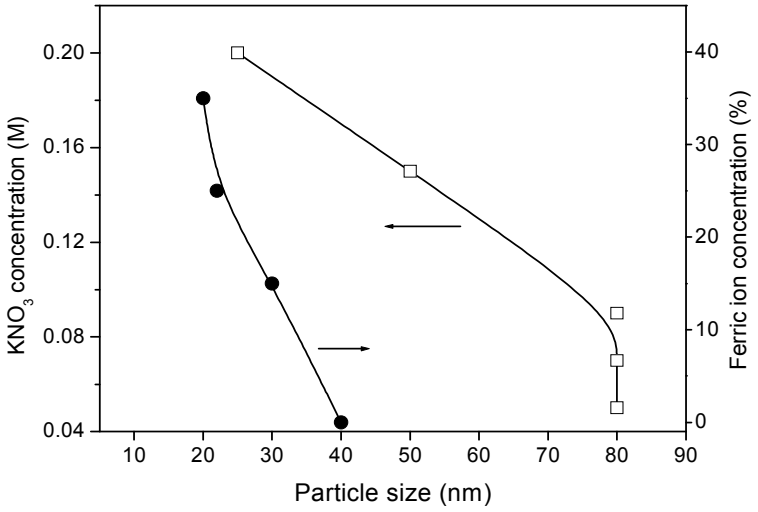

Fig. 3.1. The particle size variation with the concentration of KNO_3 and ferric ions (Connecting lines are guide to eye).

the nucleation and growth of the particles. The concentration of the ferric ions decides the number of ferrite nuclei formed which subsequently grow. Figure 3.1 shows the particle size variation with the concentration of KNO_3 and ferric ions. We shall restrict our discussions only to the ferrite nanoparticles with average particle size of 80, 50, 25 and 20 nm synthesized using 0.09 M, 0.15 M and 0.20 M of KNO_3 and 35 % ferric ions designated as sample A, B, C and D respectively for easy reference. Figure 3.2 shows the XRD of (a) sample A, (b) sample B, (c) sample C and (d) sample D. The average grain size decreases

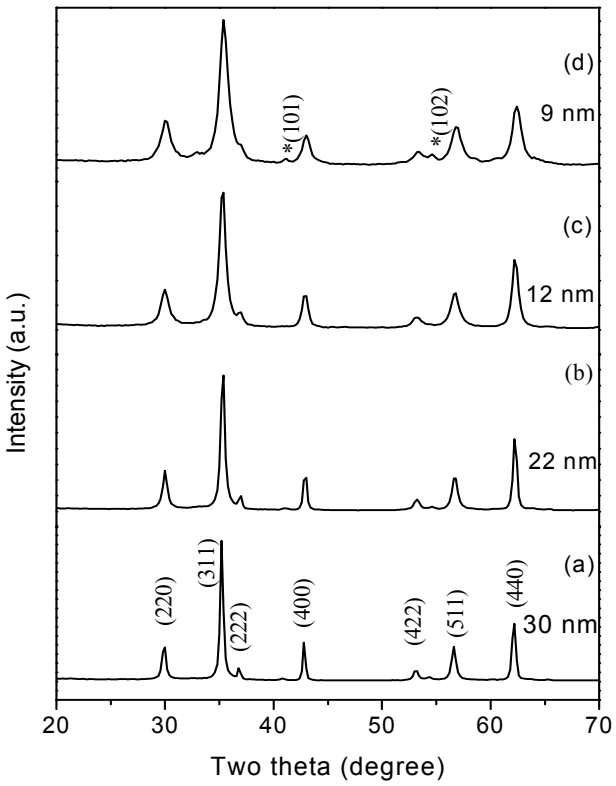

Fig. 3.2. The XRD pattern of $Mn_{0.67}Zn_{0.33}Fe_2O_4$ **(a)** sample A, **(b)** sample B, **(c)** sample C and **(d)** sample D (* represents MOOH impurity peak). The average values of the grain sizes are given in nm against each pattern.

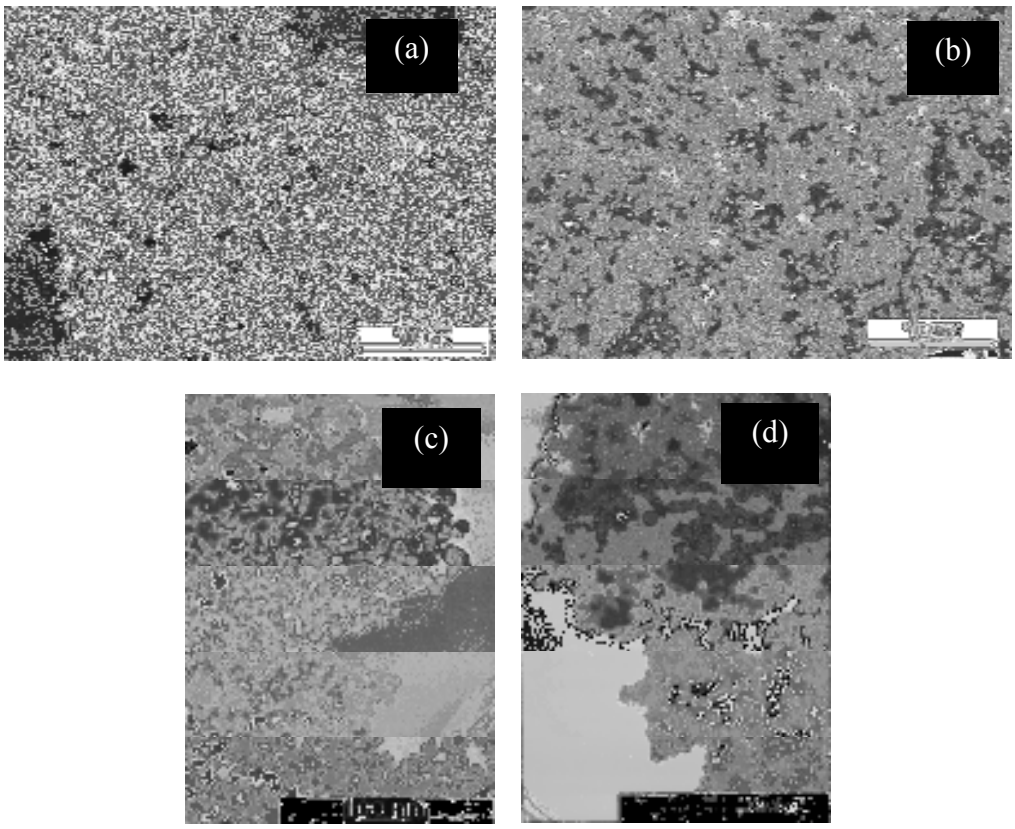

Fig. 3.3. The SEM pictures for **(a)** sample A, **(b)** sample B and TEM pictures for **(c)** sample C and **(d)** sample D.

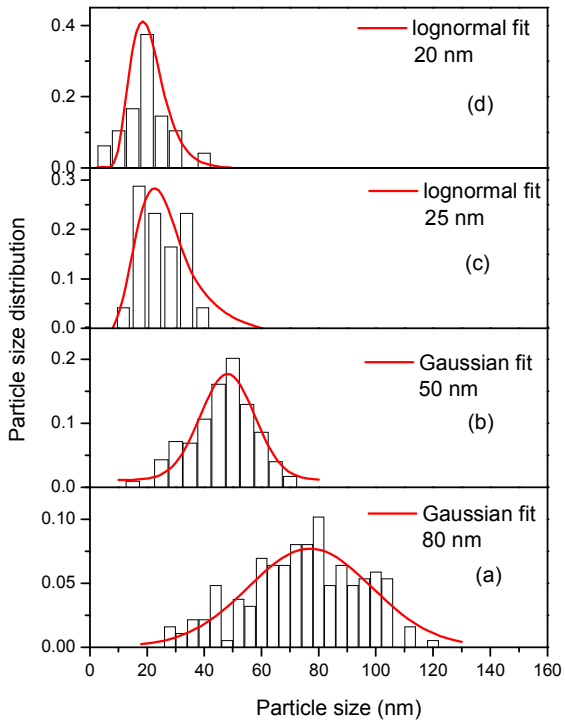

Fig. 3.4. The fitting of the particle size distribution for **(a)** sample A, **(b)** sample B, **(c)** sample C and **(d)** sample D.

from 30 nm for sample A to 22, 12 and 9 nm for samples B, C and D respectively. The formation of α-Fe_2O_3 during precipitation due to the loss of Zn^{2+} or Mn^{2+} ions has been reported for the hydrothermally synthesized [24] samples whereas only a small amount of MOOH impurity phase is present in sample D in the present study. Figs. 3.3.(a) and (b) show the SEM pictures of sample A and B and Figs. 3.3.(c) and (d) show the TEM pictures of samples C and D respectively. For the samples A and B, the average particle size was estimated to be 80 and 50 nm by fitting the particle size distribution with a Gaussian function while it was 25 and 20 nm for samples C and D respectively, as obtained from the fitting of the particle size distribution with a lognormal distribution function. These fittings for samples A, C and D are shown in Figs. 3.4.(a) – (d). The decrease in particle size for higher concentration of the oxidant is attributed to the faster oxidation of ferrous ion to ferric state and consequently an increase in the nucleation rate of ferrite nanoparticles. But lower molar concentrations of the oxidant result in a wide distribution of particle sizes with larger diameter because of the varying time intervals for nucleation according to LaMer and Dinegar [25].

3.3.2. Magnetic properties

3.3.2.1. Saturation magnetization and coercivity

Table 3.1 shows the variation of saturation magnetization, M_s and coercivity H_c of $Mn_{0.67}Zn_{0.33}Fe_2O_4$ with particle size. The saturation magnetization for the 80 nm particles was found to be 49 A m^2/kg which decreases to 34 A m^2/kg for the 20 nm particles. The decrease in saturation magnetization with the decrease in particle size is due to surface spin

Table 3.1. The variation of saturation magnetization M_s and coercivity H_c of $Mn_{0.67}Zn_{0.33}Fe_2O_4$ with particle size.

KNO_3 (M)/ Ferric ion (%) concentration	Sample (Particle size in nm)	M_s (± 2 A m^2/kg)	H_c (± 0.2 kA/m)
0.09	A (80)	49	12.5
0.15	B (50)	40	11.2
0.20	C (25)	39	1.5
35	D (20)	34	0.8

effects arising due to smaller particle sizes [26, 27]. The coercivity decreases with particle size and becomes very small for the average particle sizes of 25 nm and below, because of the presence of a considerable volume fraction of superparamagnetic particles.

3.3.2.2. No size-dependent cation distribution

Figure 3.5 shows the temperature dependent magnetization in a field of 800 kA/m for the samples A, C and D. These samples show close lying values of 632 ± 5 K, 627 ± 5 K and 634 ± 5 K respectively for their Curie temperature T_c, suggesting that there is no significant variation in the composition and also no size-dependent cation distribution. Similar results have been obtained by Jeyadevan *et al.* [28] in the case of Mn-Zn ferrite where the Curie temperature does not change with the particle size. The bulk $Mn_{0.65}Zn_{0.35}Fe_2O_4$ shows a Curie temperature of 463 K [29] whereas the Curie temperature of the nanoparticles of this ferrite is found to be as high as 723 K, which is attributed to the redistribution of the cations among the two sites [7]. The cations Fe^{3+}, Mn^{2+} and Zn^{2+} have zero crystal field stabilization energy and hence they can occupy either tetrahedral or

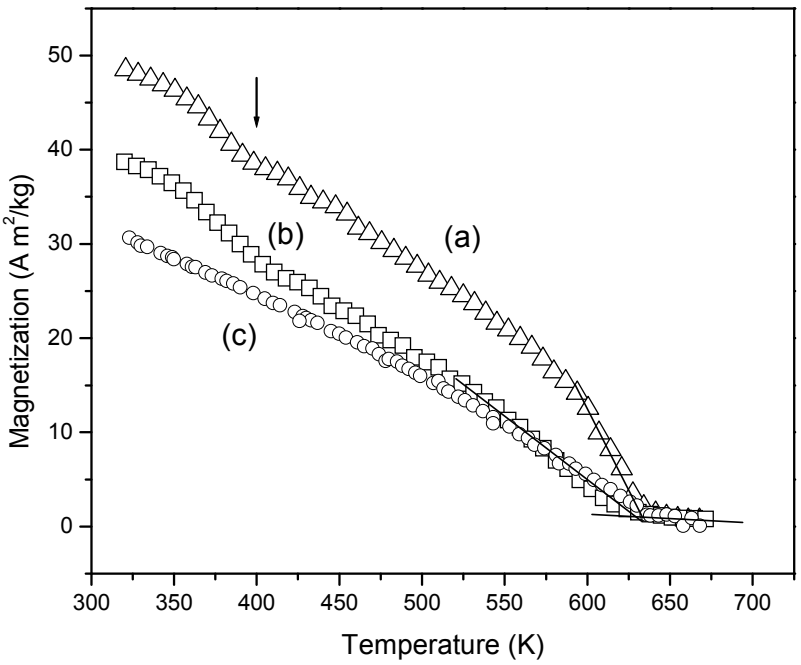

Fig. 3.5. The temperature dependent magnetization of the **(a)** sample A, **(b)** sample C and **(c)** sample D in an applied magnetic field of 800 kA/m.

octahedral sites randomly. Hence the cation distribution could vary with the method of synthesis [9, 30], which explains the observed differences in the values of T_c reported in the literature [7, 31].

3.3.2.3. Metastable cation distribution

The heating during thermomagnetic measurements can facilitate cation redistribution and hence the metastable cation distribution in the as synthesized particles starts transforming to a thermally induced stable distribution as could be easily visualized from the change in the shape of the thermomagnetization curve (a) indicated by the arrow as in Fig. 3.5. The redistribution of cations has resulted in an increase in T_c as could be visualized from the figure. Figure 3.6.(a) shows the change in the weight of the sample A as a function of temperature in the TGA experiment and (b) shows the second run for the same sample. The Curie temperature is found to be 634 K for the sample A. A broad hump is seen for the sample A at 520 K in the virgin condition whereas the hump disappears when the sample is rerun in the TGA experiment. The small increase in the weight of the sample up to 520 K during the first run is likely to be due to the possible increase in the magnetization because of the change in the cation distribution during heating. The disappearance of the hump in the second run suggests that the cation distribution had

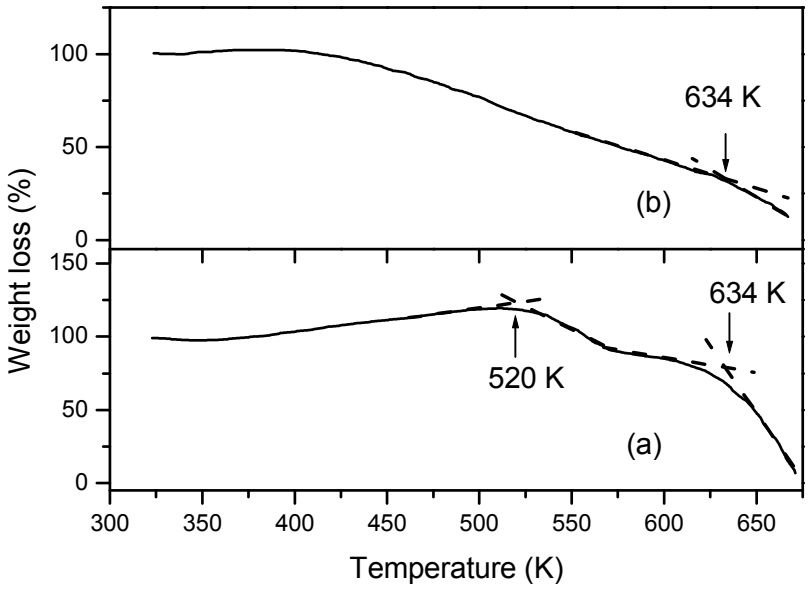

Fig. 3.6 (a) The temperature dependence of magnetization of sample A measured in a TGA and **(b)** second run for the same sample.

changed from the metastable state to the equilibrium state on heating during the first run. The above studies suggest that, in the nanocrystalline form, the cation distribution is in the metastable state whereas heating the sample takes it to the stable state.

3.3.2.4. Particle size determination using Langevin function

The distribution in the particle size affects the magnetic behaviour, as smaller particles have a relatively larger thermal energy than the anisotropic energy. The magnetic moment of the sample is given by [32]

$$\frac{M(H)}{M_s} = \int_0^\infty L(\alpha)P(r)dr \qquad (3.1)$$

where M_s is the saturation magnetization, $L(\alpha)$ is the Langevin function given by

$L(\alpha) = \coth(\alpha) - 1/\alpha$, $\alpha = \frac{VHM_s}{k_B T}$, V is the volume of the particle

and $P(r)$ is the weighting function representing the distribution in particle size. The particle size distribution is fitted with a lognormal distribution function given by

$$P(r) = \frac{1}{\sigma r\sqrt{2\pi}} \exp\left(\frac{-\ln(r/r_o)^2}{2\sigma^2}\right) \qquad (3.2)$$

where σ is the standard deviation, r is the radius and r_o is the mean radius of the particles.

The initial magnetization curve is fitted well as seen from Fig. 3.7, with Eq. (3.1) in the low-field region using the particle size distribution function given by Eq. (3.2). An average particle diameter of 25 ± 1 nm was obtained from the fitting for the sample C which agrees with the TEM results. The deviation of the Langevin fitting from the magnetization curve near the saturation region is due to the surface anisotropy of small particles [33].

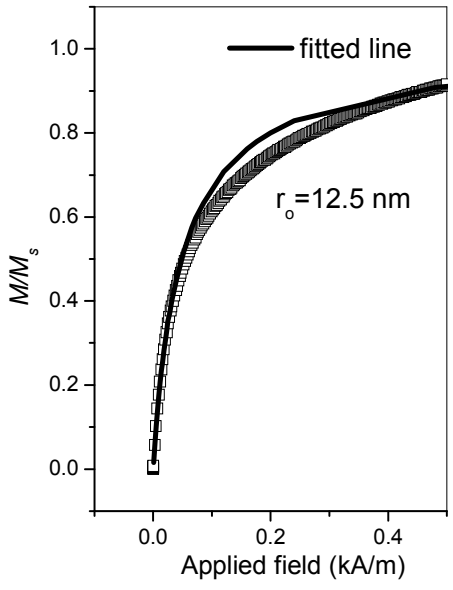

Fig. 3.7. The Langevin fit of the initial magnetization curve of sample C.

3.3.2.5. ZFC and FC measurements

Figures 3.8.(a-c) show the zero-field-cooled (ZFC) and field-cooled (FC) magnetization for samples A, C and D respectively in an applied magnetic field of 16 kA/m. The ZFC curve for sample D is almost flat below 135 K whereas for sample C it branches off from the FC value at 265 K and peaks at 165 K. The large curvature in the ZFC curve for sample A compared to that observed for the other samples suggests the presence of smaller particles with a distribution in blocking temperature. The temperature at which the ZFC and FC curves branch off represents the blocking temperature for larger particles [34, 35]. The ZFC and FC curves for sample A do not merge together at 293 K due to the presence of a large number of bigger particles with an average particle diameter of 80 nm whose blocking temperature lies above 293 K whereas for samples C and D, the separation in the curves takes place at lower temperatures due to the smaller particle sizes.

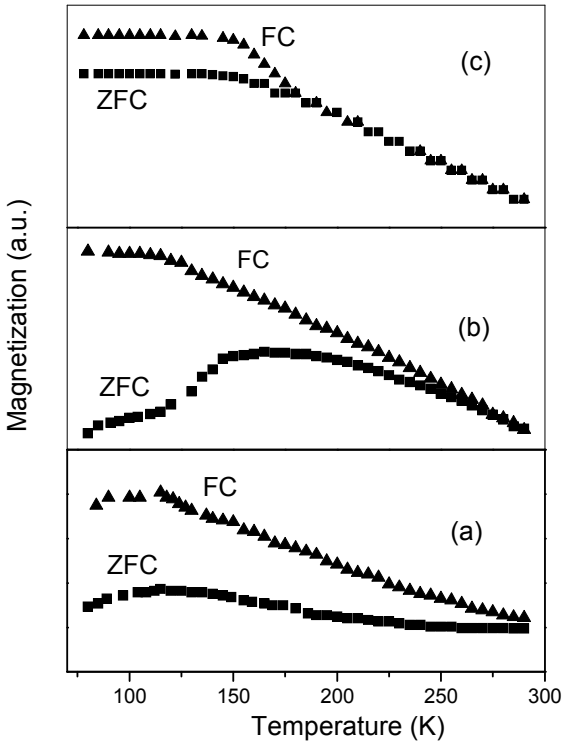

Fig. 3.8. The ZFC and FC curves for **(a)** sample A, **(b)** sample C and **(c)** sample D in an applied magnetic field of 16 kA/m.

3.3.3. Mössbauer studies

Figures. 3.9.(a)-(d) show the Mössbauer spectra at 293 K of samples A, B, C and D respectively and their corresponding Mössbauer parameters obtained from the least-squares fitting of the experimental data are shown in Table 3.2. Some of the particles in sample A, B and C are magnetically ordered as seen from the appearance of two sextets corresponding to the A- and B- sites of the spinel structure whereas all the particles in sample D are superparamagnetic at 293 K. The percentage volume of the magnetically ordered particles in samples A and B, as observed from the relative area of the sextet, is 81-82 % which

decreases to 52 % for sample C and to 0 % for sample D. The superparamagnetic doublet in sample D indicates that the blocking temperature of all the particles is below 293 K. It has been reported in the literature [36] that the superparamagnetic limit for the Mn-Zn ferrite particles is 20 nm. The coexistence of a sextet for the sample C with an average particle diameter of 25 nm and the observation of only a doublet for the sample D with an average particle diameter of 20 nm suggest that the superparamagnetic limit is around 25 nm in close agreement with the literature. The appearance of a broad sextet and a doublet for sample C indicates that the blocking temperature of the particles lies near 293 K. The hyperfine fields for the A- and B- sites are distinctly seen for the samples A and B as shown by the splitting of the sextets. The largest hyperfine field with a smaller isomer shift is characteristic of Fe^{3+} ions in tetrahedral A- site, whereas the other two sextets with

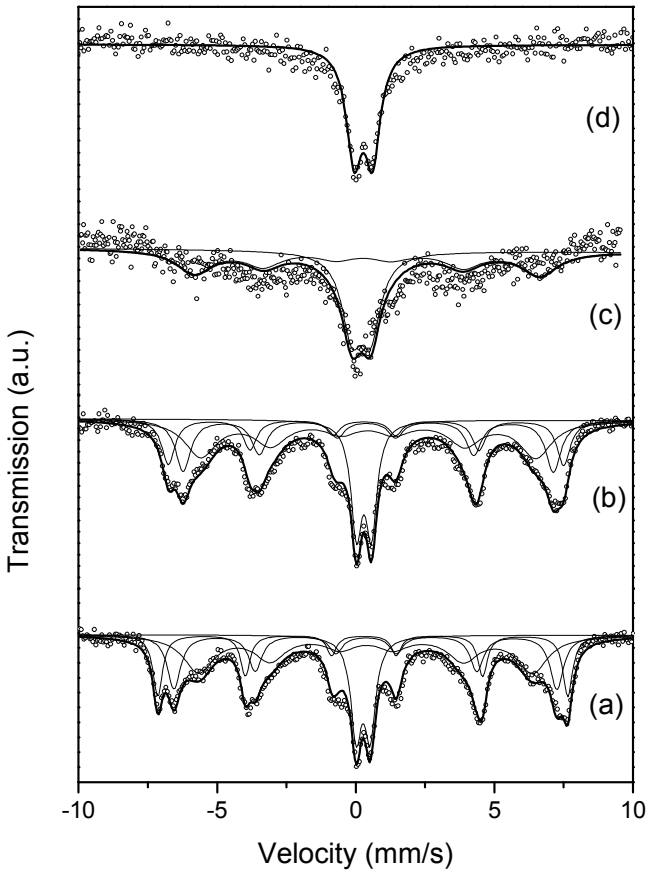

Fig. 3.9. The Mössbauer spectrum at 293 K for **(a)** sample A, **(b)** sample B, **(c)** sample C and **(d)** sample D.

Table 3.2. The Mössbauer parameters at 293 K for samples A, B, C and D.

Samples (Particle size in nm)	Hyperfine field (± 0.1 T)	Isomer shift* (± 0.05 mm/s)	Quadrupole splitting (± 0.06 mm/s)	Line width (± 0.05 mm/s)	Relative intensity (± 1%)
A	45.8	0.39	-0.04	0.41	20
(80)	42.8	0.48	0.02	0.58	24
	37.3	0.49	0.04	1.32	38
	-	0.38	0.51	0.47	18
B	44.1	0.46	0.05	0.57	19
(50)	41.1	0.53	0.06	0.65	25
	37.4	0.56	0.02	1.38	37
		0.41	0.54	0.48	19
C	38.6	0.46	0.14	1.55	52
(25)	-	0.31	0.68	0.88	48
D	-	0.39	0.67	0.68	100
(20)					

* relative to α-Fe at 293 K

relatively larger isomer shifts represent Fe^{3+} ions at two different environments in B- site. The A- site isomer shift is expected to be smaller than the B- site isomer shift due to a higher degree of covalency at A- site [37]. For sample C, because of the relaxation effects, the A- and B- site sextets are not distinctly seen and hence the Mössbauer spectrum of this sample is fitted with an average hyperfine field of 38.6 T and a superparamagnetic doublet.

Figure 3.10 shows the Mössbauer spectrum at various temperatures for sample C. The fitted Mössbauer parameters are given in Table 3.3. More and more particles are magnetically ordered as the temperature is lowered from 293 K. It is to be noted that partial magnetic ordering is seen for these particles even at 293 K as shown in Fig. 3.9.(c). A superparamagnetic doublet with a small relative intensity of 6 % is seen even at 16 K suggesting that a small volume fraction of particles with a blocking temperature less than 16 K is present in the sample which increases to 15 % at 250 K and to 48 % at 293 K. The Mössbauer spectra at 200 K and 16 K for sample D are shown in Fig. 3.11. The

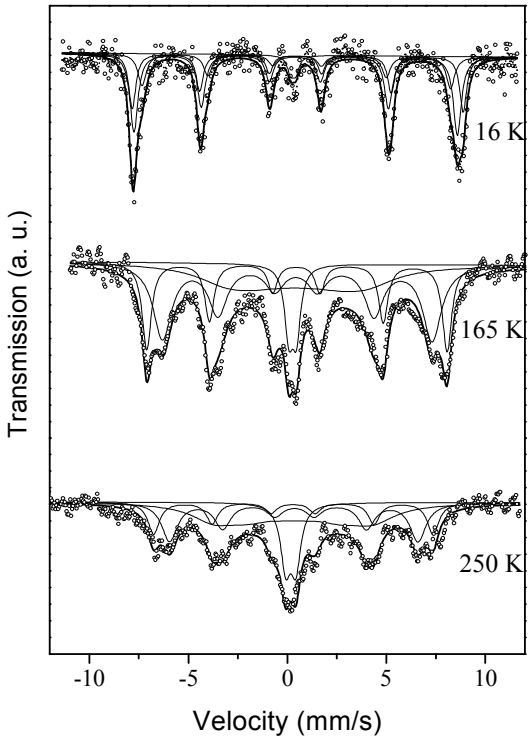

Fig. 3.10. The Mössbauer spectra of sample C at various temperatures.

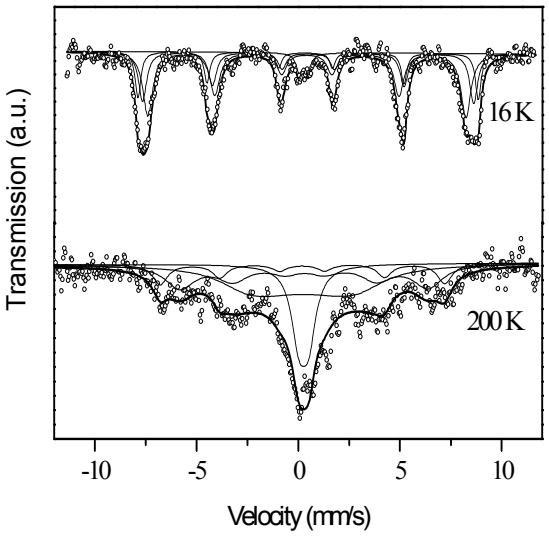

Fig. 3.11. The Mössbauer spectra of sample D at 200 K and 16 K.

Table 3.3. The Mössbauer parameters of sample C at various temperatures.

Temperature (K)	Hyperfine field (± 0.1 T)	Isomer shift* (± 0.05 mm/s)	Quadrupole splitting (± 0.06 mm/s)	Line width (± 0.05 mm/s)	Relative Intensity (± 1%)
250	43.7	0.41	0.01	0.70	18
	38.9	0.46	0.04	0.96	30
	24.7	0.43	0.02	2.82	37
	-	0.29	0.51	0.61	15
165	47.0	0.58	0.03	0.56	24
	42.2	0.58	-0.07	1.13	41
	21.9	0.60	0.02	3.62	27
	-	0.38	0.38	0.51	8
16	50.6	0.59	0.09	0.42	28
	48.4	0.55	-0.02	0.52	45
	44.8	0.63	0.07	0.83	21
	-	0.46	0.35	0.34	6

* relative to α-Fe at 300 K

Table 3.4 The Mössbauer parameters of sample D at 200 K and 16 K.

Temperature (K)	Hyperfine field (± 0.1 T)	Isomer shift* (± 0.05 mm/s)	Quadrupole splitting (± 0.06 mm/s)	Line width (± 0.05 mm/s)	Relative Intensity (± 1%)
200	43.3	0.32	0.01	0.87	13
	37.8	0.41	0.03	1.75	28
	17.3	0.33	0.01	3.32	39
	-	0.38	0.47	0.89	20
16	51.8	0.53	0.13	0.33	19
	50.4	0.59	0.01	0.47	30
	48.4	0.53	0.00	0.58	47
	-	0.37	0.44	0.38	4

* relative to α-Fe at 300 K

large linewidth of 3.32 mm/s at 200 K for the 20 nm particles represents the gradual transformation of the superparamagnetic doublet to a magnetically ordered sextet. This broad sextet with a low field for the sample D is due to the relaxation time being nearly equal to the Mössbauer time window ($\tau \approx \tau_o$) [32]. Since the direct use of ferric ions in the synthesis has resulted in a smaller particle size compared to the samples synthesized using KNO_3, the sample D has a blocking temperature which is less than 293 K. The large line width of the sextets even at 200 K is due to relaxation effects.

3.3.4. Effective magnetic anisotropy determination

The blocking temperature T_B, the temperature below which the superparamagnetic particles become magnetically ordered, is given by

$$\tau = \tau_0 \exp\left(\frac{K_{\text{eff}} V}{k_B T_B}\right) \tag{3.3}$$

where, K_{eff} is the effective magnetic anisotropy constant, V is the volume of the particle, k_B is the Boltzmann constant, τ is the relaxation time and τ_o is the relaxation time constant. The Mössbauer measurement time scale is of the order of 10^{-8} s. If the relaxation time τ, of the nanoparticles is less than τ_o, then the thermal fluctuations make the moment to fluctuate rapidly resulting in a doublet in the Mössbauer spectrum. However, as the temperature is

lowered the relaxation time (τ) increases and at the blocking temperature T_B, the relaxation time is larger than the Mössbauer time window resulting in the appearance of a sextet. Since there is always a distribution in the relaxation times due to particle size distribution, the blocking temperature is usually taken as that temperature at which the doublet and sextet intensities are equal [38]. The T_B, therefore, as measured from the Mössbauer experiments is 293 K for the sample C. Similarly T_B, from magnetic measurements (ZFC) using VSM with a measurement time of 1 s, was found to be 135 K. Using these data one could estimate the effective magnetic anisotropy constant by simultaneously solving Eq. (3.3), and it was found to be 7.78 kJ/m^3. This value is about an order of magnitude higher than that for the bulk Mn-Zn ferrite [39], with a magnetic anisotropy constant of nearly 1 kJ/m^3, which is in accordance with the values reported in the literature for other ferrites and this is attributed to the surface anisotropy of small particles [40]. The site occupancy of the cations also can influence the magnetocrystalline anisotropy as reported in the literature [41].

3.4. Conclusion

$Mn_{0.67}Zn_{0.33}Fe_2O_4$ nanoparticles with size ranging from 20 to 80 nm have been synthesized using the modified oxidation method. The Curie temperatures for all the samples are found to be within 630 ± 5 K suggesting that there is no size-dependent cation distribution. The 80 nm particles showed a magnetization of 49 A m^2/kg at 293 K which reduced to 34 A m^2/kg for the 20 nm particles. The critical particle size limit for superparamagnetism is found to be 25 nm at 293 K. The higher value of the effective magnetic anisotropy constant 7.78 kJ/m^3 for the 25 nm particles is attributed to the surface spin anisotropy of small particles.

References

[1] Q. A. Pankhrust, J. Connolly, S. K. Jones, and J. Dobson, J. Phys. D: Appl. Phys. **36** (2003) R167.

[2] P. Tartaj, M. P. Morales, S. Veintemillas-Verdaguer, T. González-Carreño, and C. J. Serna, J. Phys. D: Appl. Phys. **36** (2003) R182.

[3] C. C. Berry and A. S. G. Curtis, J. Phys. D: Appl. Phys. **36** (2003) R198.

[4] S. Mornet, S. Vasseur, F. Grasset, and E. Duguet, J. Mater. Chem. **14** (2004) 2161.

[5] V. Šepelák, U. Steinike, D. Chr. Uecker, S. Wißmann, and K. D. Becker, J. Solid State Chem. **135** (1998) 52.

[6] C. Upadhyay and H. C. Verma, Appl. Phys. Lett. **85** (2004) 2074.

[7] C. Rath, S. Anand, R. P. Das, K. K. Sahu, S. D. Kulkarni, S. K. Date, and N. C. Mishra, J. Appl. Phys. **91** (2002) 2211.

[8] A. S. Albuquerque, J. D. Ardisson, W. A. A. Macedo, and M. C. M. Alves, J. Appl. Phys. **87** (2000) 4352.

[9] B. Jeyadevan, K. Tohji, K. Nakatsuka, and A. Narayanasamy, J. Magn. Magn. Mater. **217** (2000) 99.

[10] T. Hyeon, Chem. Commun. **8** (2003) 927.

[11] Z. X. Tang, C. M. Sorensen, K. J. Klabunde, and G. C. Hadjipanayis, J. Appl. Phys. **69** (1991) 5279.

[12] M. Yokoyama, T. Sato, E. Ohta, and T. Sato, J. Appl. Phys. **80** (1996) 1015.

[13] Q. Chen and Z. J. Zhang, Appl. Phys. Lett. **73** (1998) 3156.

[14] H. Tamura and E. Matijevic, J.Coll. Interf. Sci. **90** (1982) 100.

[15] K. Nishimura, M. Abe, and M. Inoue, IEEE Trans. Magn. **38** (2002) 3222.

[16] C. N. Chinnasamy, M. Senuoue, B. Jeyadevan, O. Perales-Peres, K. Shinoda, and K. Tohji, J.Coll. Interf. Sci. **263** (2003) 80.

[17] R. H. Kodama, A. E. Berkowitz, E. J. McNiff, Jr., and S. Foner, Phys. Rev. Lett. **77** (1996) 394.

[18] A. Vega, J. Dorantes-Dávila, L. C. Balbás, and G. M. Pastor, Phys. Rev. B **47** (1993) 4742.

[19] F. Bakuzis, P. C. Moraisa, and F. Pelegrini, J. Appl. Phys. **85** (1999) 7480.

[20] L. D. Tung, V. Kolesnichenko, D. Caruntu, N. H. Chou, C. J. O'Connor, and L. Spinu, J. Appl. Phys. **93** (2003) 7486.

[21] H. S. Lee, W. C. Lee, and T. Furubayashi, J. Appl. Phys. **85** (1999) 5231.

[22] C. Cannas, G. Concas, D. Gatteschi, A. Falqui, A. Musinu, G. Piccaluga, C. Sangregorio, and G. Spano, Phys. Chem. Chem. Phys. **3** (2001) 832.

[23] M. Tada, S. Hatanaka, H. Sanbonsugi, N. Matsushita, and M. Abe, J. Appl. Phys. **93** (2003) 7566.

[24] C. Rath, K. K. Sahu, S. Anand, S. K. Date, N. C. Mishra, and R. P. Das, J. Magn. Magn. Mater. **202** (1999) 77.

[25] V. K. LaMer and R. H. Dinegar, J. Am. Chem. Soc. **72** (1950) 4847.

[26] J. M. D. Coey, Phys. Rev. Lett. **27** (1971) 1140.

[27] R. H. Kodama and A. E. Berkowitz, Phys. Rev. B **59** (1999) 6321.

[28] B. Jeyadevan, C. N. Chinnasamy, K. Shinoda, K. Tohji, and H. Oka, J. Appl. Phys. **93** (2003) 8450.

[29] J. Smith and H. P. J. Wijn, *Ferrites*, (John Wiley, New York, 1959) p. 369.

[30] S. Son, R. Swaminathan, and M. E. McHenry, J. Appl. Phys. **93** (2003) 7495.

[31] K. Tkácová, V. Šepelák, N. Števulová, and V. V. Boldyrev, J. Solid State Chem. **123** (1996) 100.

[32] S. A. Oliver, R. J. Willey, H. H. Hamdeh, and G. O. Busca, Scripta Metall. Mater. **33** (1995) 1695.

[33] M. Respaud, J. Appl. Phys. **86** (1999) 556.

[34] M. F. Hansen and S. Mørup, J. Magn. Magn. Mater. **203** (1999) 214.

[35] C. Cannas, M. F. Casula, G. Concas, A. Corrias, D. Gatteschi, A. Falqui, A. Musinu, C. Sangregorio, and G. Spano, J. Mater. Chem. **11** (2001) 3180.

[36] K. Mandal, S. Chakraverty, S. Pal Mandal, P. Agudo, M. Pal, and D. Chankravorty, J. Appl. Phys. **92** (2002) 501.

[37] N. N. Greenwood and T. C. Gibb, *Mössbauer Spectroscopy* (Chapman and Hall, London, 1971) Sec. 10.

[38] A. J. Rondinone, A. C. S. Samia, and Z. J. Zhang, Appl. Phys. Lett. **76** (2000) 3624.

[39] S. Chikazumi, *Physics of Magnetism* (Wiley, New York, 1964).

[40] B. Martínez, A. Roig, E. Molins, T. González-Carreño, and C. J. Serna, J. Appl. Phys. **83** (1998) 3256.

[41] C. N. Chinnasamy, A. Narayanasamy, N. Ponpandian, K. Chattopadhyay, K. Shinoda, B. Jeyadevan, K. Tohji, K. Nakatsuka, T. Furubayashi, and I. Nakatani, Phys. Rev. B **63** (2001) 184108.